

Article

Synthesis and Characterization of TiO₂ Nanotubes (TiO₂-NTs) with Ag Silver Nanoparticles (Ag-NPs): Photocatalytic Performance for Wastewater Treatment under Visible Light

Achraf Amir Assadi ^{1,2,3,*}, Sarra Karoui ¹, Khaled Trabelsi ⁴, Anouar Hajjaji ⁴, Walid Elfalleh ⁵ , Achraf Ghorbal ¹ , Mounir Maghzaoui ^{2,3} and Aymen Amin Assadi ^{6,*} 

- ¹ Research Unit Advanced Materials, Applied Mechanics, Innovative Processes and Environment, Higher Institute of Applied Sciences and Technology of Gabes (ISSAT), University of Gabes, Gabes 6072, Tunisia; sarra.karoui20@gmail.com (S.K.); achraf.ghorbal.issat@gmail.com (A.G.)
- ² Industries Chimiques du Fluor—Gabes Plant, 06 Rue Amine El Abbassi, Tunis 1002, Tunisia; m.maghzaoui@icf.ind.tn
- ³ Industrial Zone Gabes Port, Gabes 6071, Tunisia
- ⁴ Laboratoire de Photovoltaïque, Centre de Recherches et des Technologies de l'Énergie, Technopole de Borj-Cédria, BP 95, Hammam-Lif 2050, Tunisia; khaled0984@hotmail.com (K.T.); physicshajjaji@gmail.com (A.H.)
- ⁵ Energy, Water, Environment and Process Laboratory, (LR18ES35), National Engineering School of Gabes, University of Gabes, Gabes 6072, Tunisia; walid.elfalleh@fst.rnu.tn
- ⁶ École Nationale Supérieure de Chimie de Rennes, CNRS, ISCR (Institut des Sciences Chimiques de Rennes)—UMR 6226, Université de Rennes, F-35000 Rennes, France
- * Correspondence: achraf.assadi@gmail.com (A.A.A.); aymen.assadi@ensc-rennes.fr (A.A.A.); Tel.: +216-54-013-728 (A.A.A.); +33-22-32-38-152 (A.A.A.)



Citation: Assadi, A.A.; Karoui, S.; Trabelsi, K.; Hajjaji, A.; Elfalleh, W.; Ghorbal, A.; Maghzaoui, M.; Assadi, A.A. Synthesis and Characterization of TiO₂ Nanotubes (TiO₂-NTs) with Ag Silver Nanoparticles (Ag-NPs): Photocatalytic Performance for Wastewater Treatment under Visible Light. *Materials* **2022**, *15*, 1463. <https://doi.org/10.3390/ma15041463>

Academic Editor: Andrea Petrella

Received: 9 January 2022

Accepted: 2 February 2022

Published: 16 February 2022

Publisher's Note: MDPI stays neutral with regard to jurisdictional claims in published maps and institutional affiliations.



Copyright: © 2022 by the authors. Licensee MDPI, Basel, Switzerland. This article is an open access article distributed under the terms and conditions of the Creative Commons Attribution (CC BY) license (<https://creativecommons.org/licenses/by/4.0/>).

Abstract: In this work, we present the influence of the decoration of TiO₂ nanotubes (TiO₂-NTs) with Ag silver nanoparticles (Ag-NPs) on the photocatalysis of emerging pollutants such as the antibiotic diclofenac sodium. The Ag-NPs were loaded onto the TiO₂-NTs by the anodization of metallic titanium foils. Diclofenac sodium is an emerging pollutant target of the pharmaceutical industry because of its negative environmental impact (high toxicity and confirmed carcinogenicity). The obtained Ag-NP/TiO₂-NT nanocomposites were characterized by X-ray diffraction (XRD), photoluminescence spectroscopy (PL), scanning electron microscopy (SEM), transmission spectroscopy (TEM), and X-ray photoelectron spectroscopy (XPS). In order to study the photocatalytic behavior of Ag-NPs/TiO₂-NTs with visible cold LEDs, the possible photocatalytic mechanism of antibiotic degradation with reactive species (O₂^{•−} and OH[•]) was detailed. Moreover, the Langmuir–Hinshelwood model was used to correlate the experimental results with the optimized catalyst. Likewise, reuse tests showed the chemical stability of the catalyst.

Keywords: Ag-NPs/TiO₂ nanotubes; batch reactor; wastewater treatment; reactive species; kinetic modeling

1. Introduction

Pharmaceuticals are undoubtedly one of the major advances in modern medicine. Nowadays, they are widely prescribed in humans and animals, both for curative and preventive purposes. However, excessive use can lead to the emergence of resistant bacteria through mechanisms such as (i) enzymatic degradation of antibacterial drugs, (ii) alteration of bacterial proteins that are antimicrobial targets, and (iii) modification in membrane permeability to antibiotics [1–3]. In addition, these substances are not completely metabolized by organisms. The immediate consequence is that a certain unmetabolized amount ends up directly in the soil and in surface water [4,5].

Thus, the sources of pharmaceutical substances in the environment are hospital and domestic discharges, which end up in wastewater treatment plants where they are not

completely degraded and therefore discharged into surface water. The concentrations in the receiving environment can thus vary according to the biodegradability of the molecules as well as the capacity of the water treatment stations to eliminate or transform them, as these are designed and mainly sized to treat the so-called physicochemical parameters “conventional” (suspended solids, BOD₅, DCO, nitrogen, phosphorus) [5]. The immediate consequence of such a situation is that for the past fifteen years, drug residues have been found in river water because some treatment plants are still not equipped with effective processes to retain or degrade them [6–10].

To date, several emerging and promising technologies provide a solution to this problem. Among these, the heterogeneous photocatalysis with visible light reveals interesting prospects in terms of degradation/mineralization of compounds, with low energy consumption. Recent studies on model pharmaceutical compounds indicate that this technology has been explored and developed.

In the past decade, titanium dioxide (TiO₂) has been one of the most studied materials thanks to its unique chemical and physical properties, including its high chemical stability, high resistance to photo corrosion, and its low cost [11]. Nanostructured TiO₂ has also been used in many applications such as sensors [12], photocatalysis [13–16], and solar energy conversion [17]. TiO₂ nanotubes have attracted particular attention because of their high specific surface area [18], high photoactivity [19], and the rapid transfer rate of holes and electron–hole pairs (e[−]/h⁺) photogenerated along the nanotubes [20–22]. However, two major factors limit the performance of TiO₂. On the one hand, due to its wide forbidden energy band (3.2 eV for anatase TiO₂), the optical absorption of TiO₂ is limited to the UV spectrum. On the other hand, the photogenerated (e[−]/h⁺) pairs exhibit a high rate of recombination due to a high density of crystal defects [23]. To overcome these problems, many strategies have been established, such as doping TiO₂ (metallic or non-metallic dopants) [13,17] and coupling with other semiconductors [19,20,24], which could expand absorption under visible light and improve the lifetime of the photogenerated (e[−]/h⁺) pairs. Recently, it has been shown that the decoration of TiO₂ nanotubes with noble metal nanoparticles can increase their absorption in the visible range, thanks to the surface plasmon resonance (SPR) [25] induced in the metallic nanoparticles in the presence of a light wave. The SPR of the noble metal can be adjusted by controlling the size, shape, and dispersion of the nanoparticles. Nanoparticles of silver (Ag) are used to improve the photoactivity of TiO₂ nanotubes due to the favorable arrangement of the energy level, which allows the electrons excited by SPR on the Ag nanoparticles to be transferred into the TiO₂ nanotubes in the presence of visible light. In addition, chemical pathways have been used to decorate TiO₂ nanotubes with Ag nanoparticles. However, using these techniques cannot control the size and shape of Ag nanoparticles, which can easily accumulate. In addition, the organic agents employed in the growth of Ag nanoparticles can affect the electrical and optical properties of the composite.

In this work, Ag nanoparticles were deposited onto TiO₂ nanotubes using the photoreduction process, which allows the size of nanoparticles to be controlled by adjusting the UV irradiation time. TiO₂ nanotubes decorated with Ag nanoparticles were used as photoanodes in a photoelectrochemical system, showing a significant improvement in photo-conversion efficiency. Moreover, nanotubes (TiO₂-NTs) decorated with Ag silver nanoparticles (Ag-NPs) were used for the photocatalytic degradation of emerging pollutants, such as the antibiotic diclofenac sodium, with visible cold LEDs.

2. Setup

The samples were 99.99% purity metal (Ti) plates with a surface area of 2 × 1.5 cm² and a thickness of approximately 0.5 mm. They had identical characteristics to maximize the probability of the same results. In order to achieve surface activation and to avoid any adhesion problems, the samples were first polished using abrasive papers with different grain sizes: 320, 400, 600, 800, 1000, 1200, and 2000. Next, the samples were rinsed with acetone, ethanol, and then bi-distilled water for 10 min in an ultrasonic bath to remove

impurities and foreign materials introduced in the polishing step. Finally, the samples were air-dried for some time. Electrochemical experiments were conducted in the laboratory at room temperature. All samples were prepared by anodic oxidation under identical experimental conditions. This was performed in an electrolyte cell containing 100 mL ethylene glycol, 1% ammonium fluoride (NH_4F), and 2% water (H_2O). The anodization was 120 min in duration under a fixed voltage of 60 V at a temperature maintained at approximately 25 °C. The samples obtained were calcined for 1 h at 400 °C.

The photoreduction method consists of immersing the TiO_2 nanotubes in a solution of silver nitrate (AgNO_3) of 0.1 M concentration for 24 h in the dark to allow the silver ions to be adsorbed on the TiO_2 surface. Afterward, the samples were rinsed with water and then immersed in methanol under UV illumination ($\lambda = 256 \text{ nm}$) for 10 and 20 min. Under the effect of UV radiation, silver ions (Ag) reduce to metallic form. By increasing the UV irradiation time, Ag nanoparticles increase in size and form agglomerates [1].

The synthesized catalysts were placed in Petri dishes containing the antibiotic solution to be treated. The catalysts were illuminated by visible cold LEDs. This experimental setup is shown in Figure 1. Antibiotic concentration was also monitored by spectrophotometry at 270 nm.

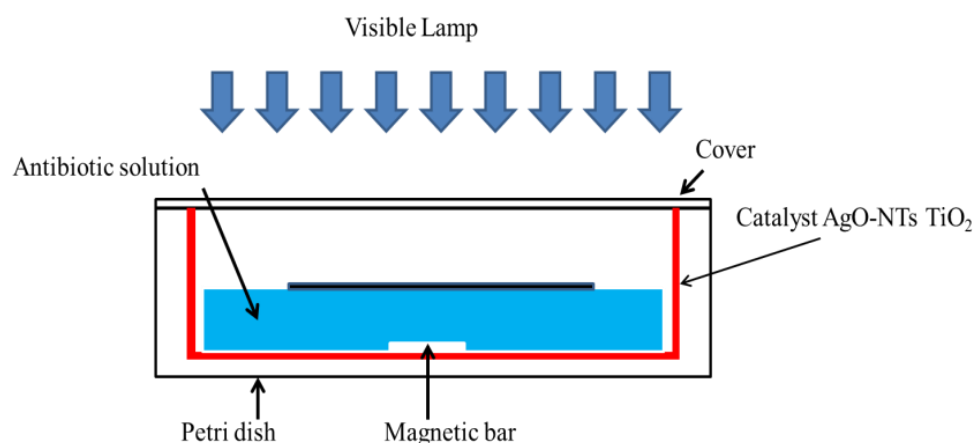


Figure 1. The micro-reactor in a Petri dish used for the treatment of antibiotics by photocatalysis.

Photo-degradation experiments were performed in order to estimate the catalytic efficiencies of TiO_2 -NTs and Ag-NPs/ TiO_2 -NTs at various deposition times (10 min, 20 min). The experimental setup consisted of the catalysts (dimensions: $1.2 \times 2.5 \text{ cm}$) placed in the photocatalytic batch reactor. An initial antibiotic concentration of 1 mg/L was studied. The lamp was lighted after reaching the adsorption–desorption equilibrium between the catalyst and the antibiotic. For this reason, the reactor containing the assembly was kept in the dark for 1 h before lighting the lamp.

3. Results and Discussion

3.1. Characterizations of Ag-NPs/ TiO_2 -NTs

Scanning electron microscopy (SEM, TESCAN VEGA3) was carried out to visualize the nanostructured morphologies of samples. The elemental analysis of samples was determined by energy-dispersive X-ray spectroscopy (EDS). The TEM and HRTEM images were obtained with the FEI Tecnai G20 microscope operating at 200 kV and equipped with the LaB6 filament. The X-ray photoelectron spectroscopy (XPS) measurements were carried out using a Jeol JPS-9200 photoelectron spectrometer with an achromatic Mg/Al X-ray source at 500 W. The spectra excitations were performed using Mg $\text{K}\alpha$ radiation (1253.6 eV). During XPS data acquisition, the C1s (285.0 eV) peak was used as a reference to correct XPS data from sample charging. The X-ray diffractometer (Cu $\text{K}\alpha$ radiation, $\lambda = 1.5406 \text{ \AA}$, PANalytical B.V., Almelo, The Netherlands) was used to identify the crystalline structure and the Pt nanoparticles phase. The photoluminescence (PL) spectra were recorded with a

PerkinElmer spectrophotometer equipped with a xenon lamp at an excitation wavelength $\lambda = 340$ nm.

Scanning Electron Microscopy (SEM)

Figure 2 shows SEM images of TiO₂ nanotubes decorated with Ag nanoparticles obtained with 10 min and 20 min pulse durations. The TiO₂-NTs, without metallic nanoparticles, were vertically aligned on titanium substrates. These nanotubes had a diameter of around 100 nm and a length of around 15 μ m (inset Figure 2a). We note the presence of small, uniformly dispersed Ag nanoparticles, and a few aggregates at the top of the nanotubes. The images show a nano-tubular structure with an average diameter of 150 nm. The Ag nanoparticles are very small in size, so they are not observable with SEM.

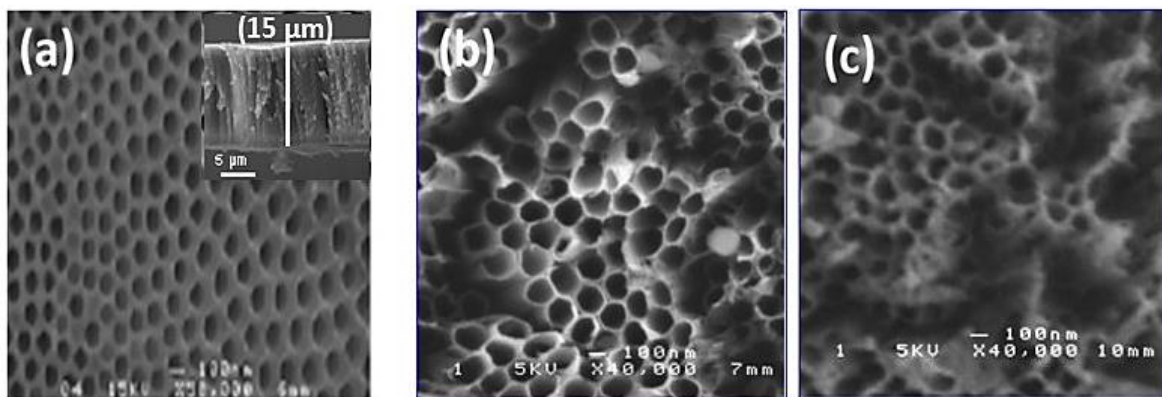


Figure 2. Typical SEM images of TiO₂-NTs (a) before and (b) after their Ag-NPs decoration at 10 min and (c) 20 min.

The chemical composition of TiO₂ nanotubes decorated with Ag nanoparticles was estimated by EDX. Figure 3 shows the EDX spectra of TiO₂ nanotubes decorated with Ag nanoparticles; the atomic percentage of silver increases with photo-reduction time: 0.2 at. % for 10 min Ag/TiO₂ and 0.3 at. % for 20 min Ag/TiO₂.

The TiO₂-NTs adorned with Ag-NPs were examined by TEM (Figure 4) to verify the presence of Ag-NPs in the TiO₂-NTs. A drop of Ag-NPs/TiO₂-NTs dispersed in solution was applied to the TEM holey carbon grids.

Figure 4a reveals the presence of arbitrary shapes of Ag-NPs on the TiO₂-NTs' surface.

Figure 5 shows the X-ray diffractograms of pure TiO₂ nanotubes decorated with Ag nanoparticles annealed at 400 °C. All samples crystallized in the anatase structure.

Here, we note that the preferential orientation peak (101) characteristic of the anatase phase of titanium oxide continues to decrease with the increase in the deposition time of silver nanoparticles on TiO₂ nanoparticles. In addition, it is noted that all the samples crystallize in the anatase structure, and the additional peaks characterizing Ag can only be observed from the diffractogram of the TiO₂-NTs decorated with silver NPs at 20 min; they cannot be observed for the deposition time of less than 10 min. Indeed, below 20 min of UV irradiation, the amount of Ag incorporated is too low to be detected by this characterization technique.

As can be seen in Figure 6, the formation of Ag species was confirmed by the XPS results. Figure 6a exhibits an O1s peak at 530.8 eV, attributed to the oxide. The appearance of the Ti-2p peak position at a binding energy of 459 eV (Figure 6b) proved that the main chemical valence of Ti is +4. This finding corroborates the assigned values for anatase TiO₂ in the NIST database. Figure 6c shows the typical XPS signature of the Ag 3d doublet (3d_{5/2} and 3d_{3/2}) taken from the surface of the TiO₂-NTs decorated with Ag-NPs. The signals at 374.3 and 368.3 eV are attributed to Ag 3d_{3/2} and Ag 3d_{5/2} of Ag-NPs, respectively.

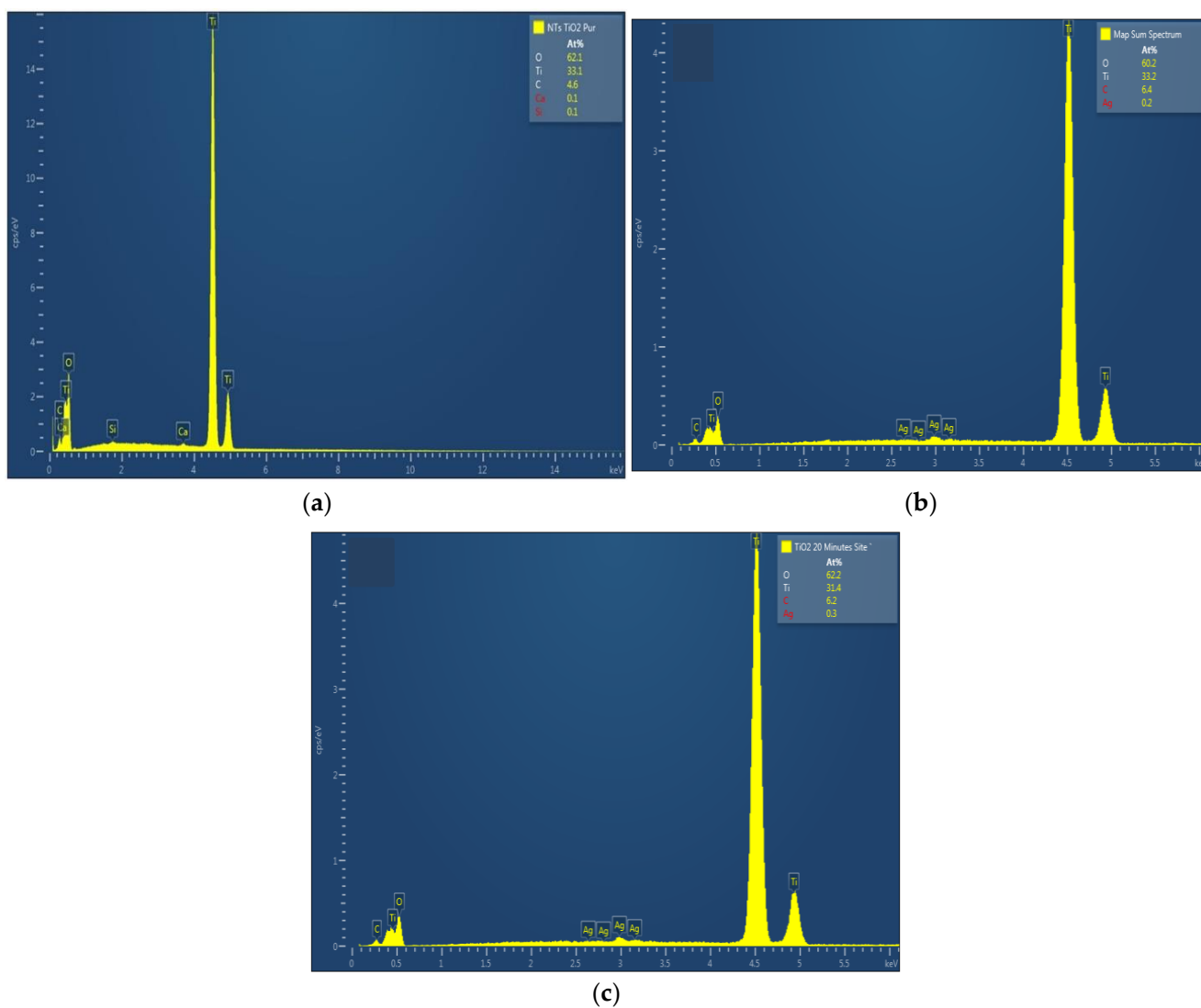


Figure 3. EDX spectra of TiO₂ nanotubes decorated with silver nanoparticles: (a) undecorated TiO₂-NTs, (b) 10 min Ag-NPs/TiO₂-NTs, and (c) 20 min Ag-NPs/TiO₂-NTs.

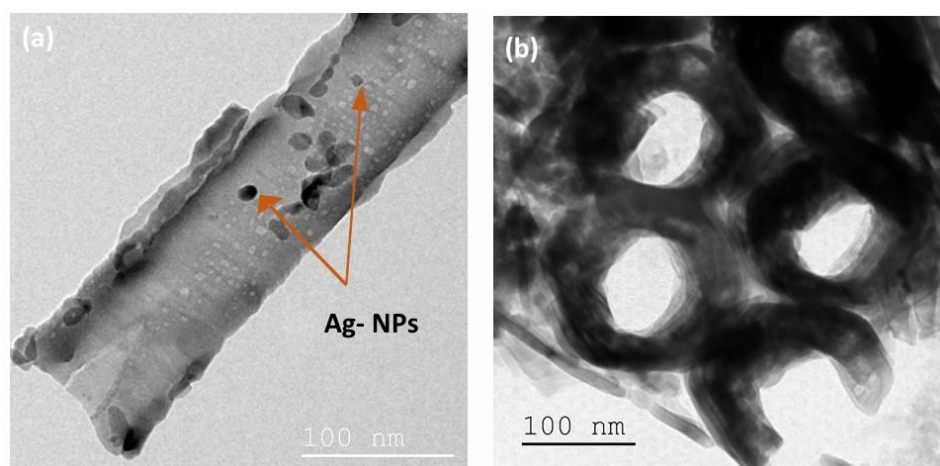


Figure 4. (a) Top view and (b) cross-section TEM images of Ag-NPs (20 min)/TiO₂-NTs array.

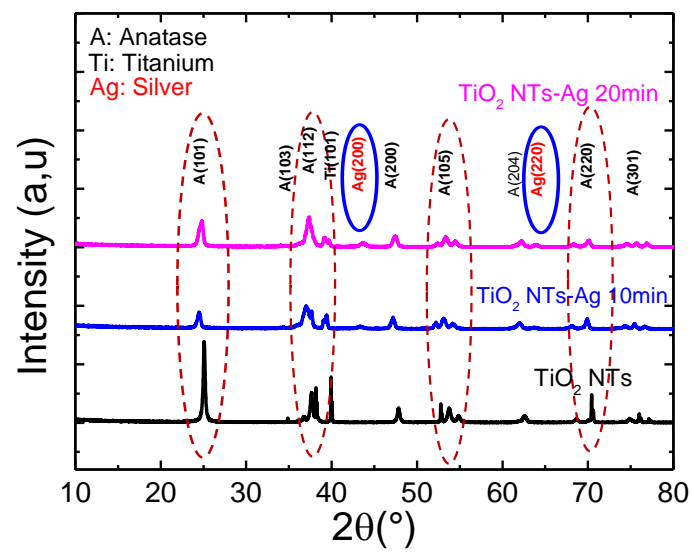


Figure 5. X-ray diffractogram of pure TiO_2 nanotubes decorated with silver nanoparticles.

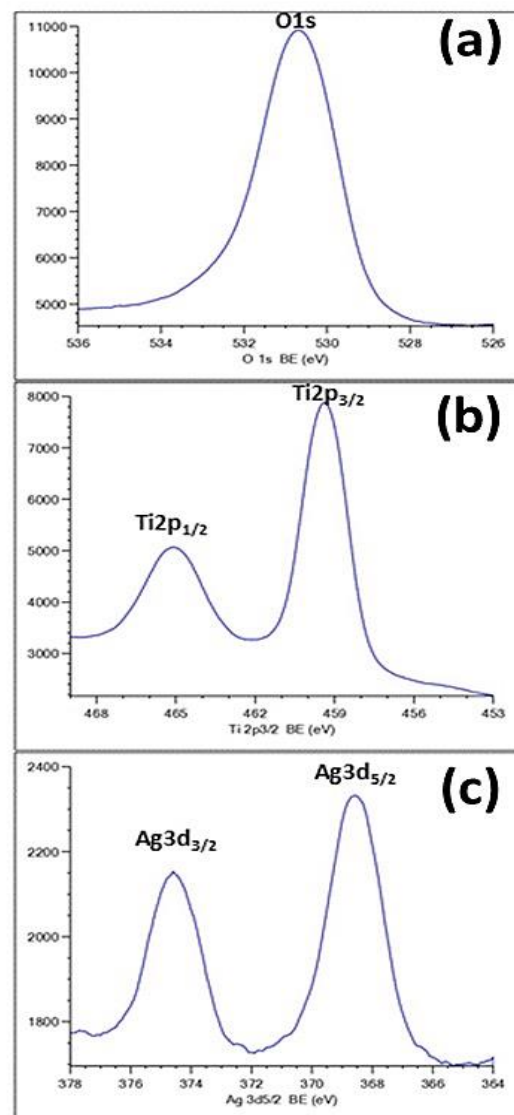


Figure 6. XPS spectra of Ag-NPs (20 min)/ TiO_2 -NTs: (a) O1s; (b) Ti2p; (c) Ag 3d.

These energies often correspond to the metal silver [26], proving the fully metallic character of the used Ag-NPs. This result confirms the effectiveness of the photoreduction process used in the preparation step.

The photoluminescence (PL) of TiO₂-NTs can inform us about the lifespan and transport of photogenerated charges. Figure 7 shows the photoluminescence spectra of pure TiO₂-NTs decorated with Ag-NPs. The peak located at 365 nm (3.4 eV) is attributed to the electron transition between the valence and conductive bands of TiO₂. The peaks present at 459 nm, 483 nm, and 531 nm are attributed to the oxygen vacancies present on the surface of TiO₂ [27,28].

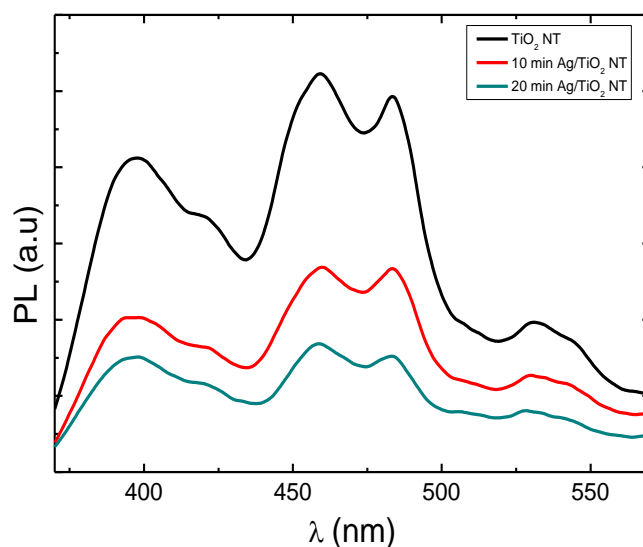


Figure 7. Photoluminescence spectra of pure TiO₂ nanotubes decorated with silver nanoparticles.

TiO₂-NTs decorated with Ag-NPs exhibit a lower PL intensity compared to that of pure TiO₂, which shows that Ag nanoparticles reduce the density of radiative recombination centers (luminescent centers). This result can be explained by the migration of electrons photogenerated under UV radiation ($\lambda_{\text{excitation}} = 340 \text{ nm}$) from the conduction band towards Ag nanoparticles, thus reducing radiative recombination within TiO₂ [29].

3.2. Photocatalytic Experiments

3.2.1. Effect of Silver Decoration

The photocatalytic performances of Ag-NP/TiO₂-NT catalysts were estimated by photocatalytic degradation of the antibiotic under visible light irradiation at ambient temperature. Figure 8 shows the pollutant removal using Ag-NPs/TiO₂-NTs decorated by photoreduction for 10 and 20 min. It is seen from Figure 8 that the pollutant removal was pertinently affected by the different decoration times. In this test, it is readily seen that the concentrations of pollutants decreased over time under visible light irradiation. Moreover, a decoration of Ag in 10 min increased the pollutant removal from 35% to 80% of the initial concentration of 2.5 mg/L. This enhancement is related to the availability of the generated active sites at the interface of the catalyst deposited at 10 min [30]. However, the pollutant degradation will tend to be limited at high time values, because these values are too high to form multiple layers of catalysts, thus generating different ions and charges, which leads to distinguished charges at the interfaces of thin films and coverage of all TiO₂-NTs.

3.2.2. Effect of Inlet Concentration: Kinetic Modeling

A representation of the change in concentration over time for four initial concentrations is shown in Figure 9a. As was observed, the increase in the concentration generally favors the pollutant degradation.

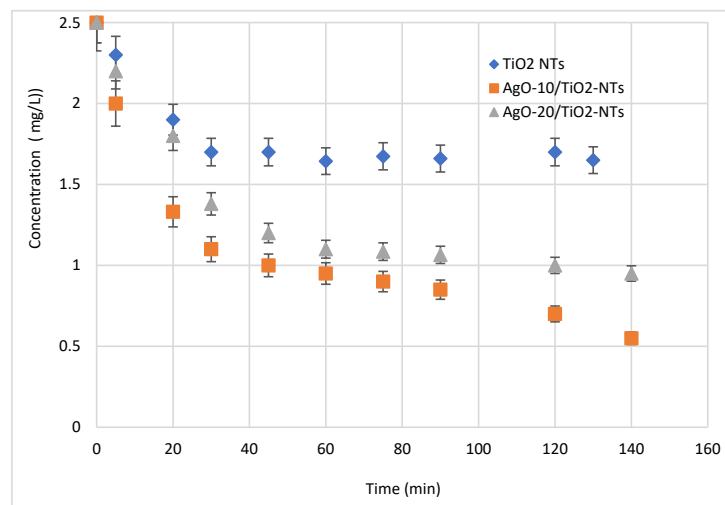
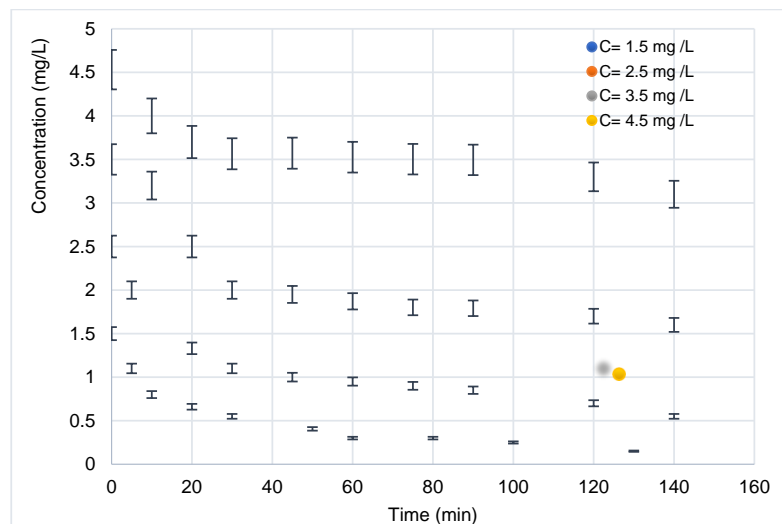
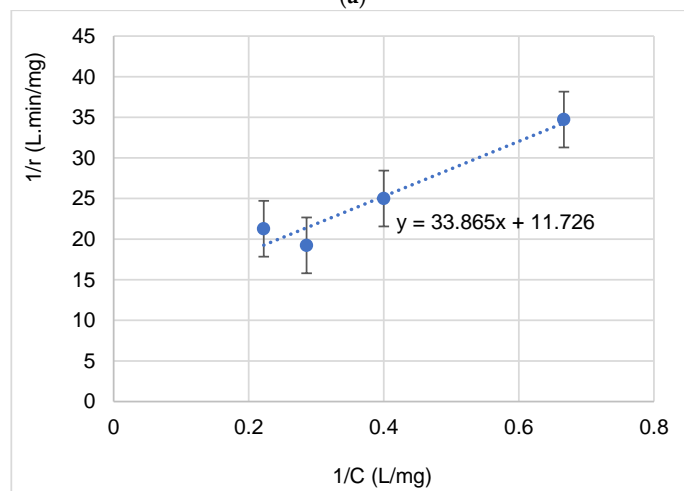


Figure 8. Effect of decoration of Ag-NPs on the photocatalytic activity of the Ag-NP/TiO₂-NT photocatalyst.



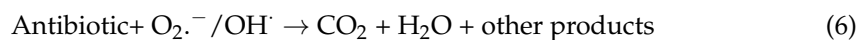
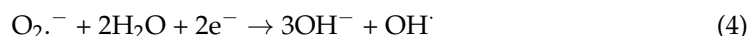
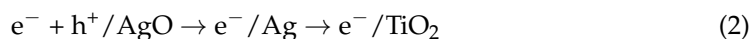
(a)



(b)

Figure 9. (a) Evolution of the concentration of the diclofenac antibiotic during its photocatalytic degradation as a function of time for 4 initial concentrations. (b) Linearization of the Langmuir-Hinshelwood isotherm during the degradation of the antibiotic (calculation of k_c and K constants).

At low concentrations, the kinetics are faster [31]. This can be explained by the fact that more molecules are “available” in the solution and that visible light accesses the surface of the catalyst more easily, which leads to an increase in the speed of photocatalytic degradation [32–35]. However, at high concentrations, molecules begin to act as a filter for incident visible light, so that light hardly reaches the surface of the TiO₂, resulting in slower photocatalytic degradation [28,36–40]. This same trend has been observed by [41]. Under visible light, electron–hole pairs were produced in the valence bands (VB) of AgO and TiO₂. Then, the photo-generated electrons passed from the valence bands to their conduction bands (CB). At the same time, electrons can be rapidly transferred to the semiconductor (TiO₂) interface, which has been reported in Au core–Cu₂O shell particles [21,25]. This could be due to the fact that the heterojunction in Ag–AgO/TiO₂ assisted the transfer of photo-generated electrons and holes. Thus, these electrons can quickly be transferred into the TiO₂ interface and then undergo a transformation, as described below [21].



To describe the Ag (10 min)/TiO₂-NTs' catalytic performance, the Langmuir–Hinshelwood (L-H) model was used [42]:

$$r_0 = -\frac{d[\text{pollutant}]}{dt} = k_c \frac{K[\text{pollutant}]_0}{1 + K[\text{pollutant}]_0} \quad (7)$$

where r_0 (mg·L⁻¹ min⁻¹) is the initial photodegradation rate, $[\text{pollutant}]_0$ is the initial BUT concentration (mg/L), K is the adsorption constant (L/mg), and k_c is the kinetic constant (mg·L⁻¹ min⁻¹) at maximum coverage of the experimental conditions.

The plot of $1/r_0$ versus $1/[\text{pollutant}]_0$ (Figure 9b) allows determining k_c and K values. The linearized (L-H) equation is:

$$\frac{1}{r_0} = \frac{1}{k_c K} \times \frac{1}{[\text{pollutant}]_0} + \frac{1}{k_c} \quad (8)$$

Table 1 illustrates the kinetic and adsorption constants of L-H.

Table 1. L-H constants (k_c and K) on the 10 min AgO-NPs/TiO₂-NT catalyst.

k_c : Kinetic Constant of L-H (mg/(L·min))	K : Adsorption Constant of L-H (L/mg)
2.9×10^{-3}	2.88

3.3. Catalyst Reusability

Catalyst reusability is a major issue to look into because it measures how well a catalyst can degrade contaminants in solution. Therefore, several visible photocatalytic experiments were performed to examine the ability of the elaborated silver sample to degrade antibiotics in four successive cycles.

After each degradation cycle, the 10 min Ag-NPs/TiO₂-NTs were well washed and reused. The photocatalytic findings of repetitive use (four cycles) of the 10 min Ag-NP/TiO₂-NT photocatalyst are shown in Figure 10. Figure 10 shows no loss of sample photoactivity. These results prove the overall potential of the 10 min Ag-NP/TiO₂-NT catalyst for water treatment applications. Generally, the same slope is noted in each cycle. Consequently, these

results shown below prove the availability of active sites and the excellent photocatalytic stability of this catalyst.

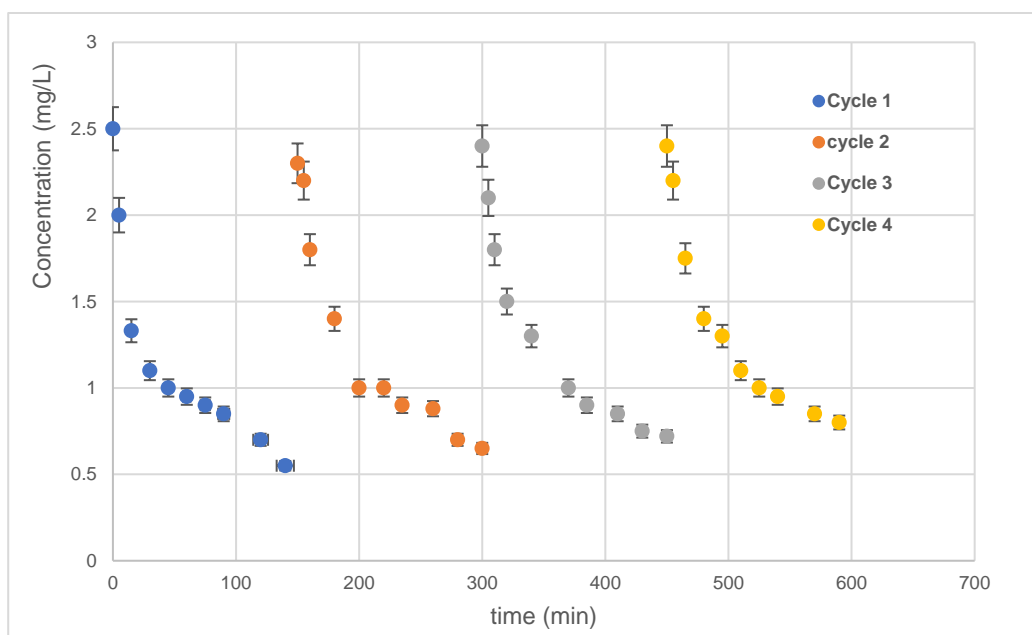


Figure 10. Four successive cycles of photocatalytic oxidations using the 10 min Ag-NP/TiO₂-NT catalyst.

4. Conclusions

The titanium electrochemical anodization and the photochemical reduction of Ag-NPs on TiO₂-NTs were successfully used to create the Ag-NP/TiO₂-NT nanocomposites. Homogeneous nanotubes with a diameter of 100 nm were used to synthesize TiO₂-NTs, which were then crystallized in the anatase phase. The Ag-NP deposition was performed at various electrodeposition times. The Ag-NPs' adjunction to the TiO₂-NTs increased the visible light absorption until almost 500 nm. Antibiotic removal experiments were conducted by TiO₂-NTs and Ag-NPs/TiO₂-NTs with various photoreduction times under visible light (380–720 nm). These tests revealed a high photocatalytic efficiency. This finding can be explained by the combination of the energy band level positions of semiconductors and the high visible light absorption of Ag nanoparticles. The Ag-NP/TiO₂-NT photocatalytic system significantly improved the antibiotic degradation concerning the TiO₂-NTs alone, because of the extended photoresponse and the efficient photogeneration of electron–hole pairs under UV/visible light. Thus, this work shows the high stability of the Ag-NP/TiO₂-NT nanocomposites under UV light irradiation.

Author Contributions: A.A.A. (Achraf Amir Assadi) and S.K.: validation, investigation, visualization, resources, writing—original draft, writing—review and editing; K.T. and A.H.: conceptualization, validation, writing—original draft, writing—review and editing, visualization, supervision; W.E. and A.A.A. (Aymen Amin Assadi): methodology, validation, investigation, writing—review and editing; A.G. and M.M.: conceptualization, methodology, supervision. All authors have read and agreed to the published version of the manuscript.

Funding: This project was carried out under the MOBIDOC scheme, funded by the Tunisian Ministry of Higher Education and Scientific Research through the PromESSE project and managed by the ANPR.

Informed Consent Statement: Not applicable.

Data Availability Statement: Not applicable.

Conflicts of Interest: The authors declare no conflict of interest.

References

1. Assadi, A.A.; Bouzaza, A.; Vallet, C.; Wolbert, D. Use of DBD plasma, photocatalysis, and combined DBD plasma/photocatalysis in a continuous annular reactor for isovaleraldehyde elimination—Synergetic effect and byproducts identification. *Chem. Eng. J.* **2014**, *254*, 124–132. [[CrossRef](#)]
2. Baaloudj, O.; Assadi, I.; Nasrallah, N.; El, A.; Khezami, L. Simultaneous removal of antibiotics and inactivation of antibiotic-resistant bacteria by photocatalysis: A review. *J. Water Process Eng.* **2021**, *42*, 102089. [[CrossRef](#)]
3. Kenfoud, H.; Nasrallah, N.; Baaloudj, O.; Meziani, D.; Chaabane, T.; Trari, M. Photocatalytic reduction of Cr(VI) onto the spinel CaFe₂O₄ nanoparticles. *Optik* **2020**, *223*, 165610. [[CrossRef](#)]
4. Boyjoo, Y.; Sun, H.; Liu, J.; Pareek, V.K.; Wang, S. A review on photocatalysis for air treatment: From catalyst development to reactor design. *Chem. Eng. J.* **2017**, *310*, 537–559. [[CrossRef](#)]
5. Baaloudj, O.; Nasrallah, N.; Kenfoud, H.; Algethami, F.; Modwi, A.; Guesmi, A.; Assadi, A.A.; Khezami, L. Application of Bi₁₂ZnO₂₀ Sillenite as an Efficient Photocatalyst for Wastewater Treatment: Removal of Both Organic and Inorganic Compounds. *Materials* **2021**, *14*, 5409. [[CrossRef](#)]
6. Asadi-Ghalhari, M.; Mostafaloo, R.; Ghafouri, N.; Kishipour, A.; Usei, S.; Baaloudj, O. Removal of Cefixime from aqueous solutions via proxy electrocoagulation: Modeling and optimization by response surface methodology. *React. Kinet. Mech. Catal.* **2021**, *134*, 459–471. [[CrossRef](#)]
7. Baaloudj, O.; Nasrallah, N.; Bouallouche, R.; Kenfoud, H. High efficient Cefixime removal from water by the sillenite Bi₁₂TiO₂₀: Photocatalytic mechanism and degradation pathway. *J. Clean. Prod.* **2022**, *330*, 129934. [[CrossRef](#)]
8. Almansba, A.; Kane, A.; Nasrallah, N.; Wilson, J.M.; Maachi, R.; Lamaa, L.; Peruchon, L.; Brochier, C.; Amrane, A.; Assadi, A.A. An engineering approach towards the design of an innovative compact photo-reactor for antibiotic removal in the frame of laboratory and pilot-plant scale. *J. Photochem. Photobiol. A Chem.* **2021**, *418*, 113445. [[CrossRef](#)]
9. Bourkeb, K.; Baaloudj, O. Facile electrodeposition of ZnO on graphitic substrate for photocatalytic application: Degradation of antibiotic in a continuous stirred-tank reactor. *J. Solid State Electrochem.* **2022**, *26*, 573–580. [[CrossRef](#)]
10. Ochiai, T.; Fujishima, A. Photoelectrochemical properties of TiO₂ photocatalyst and its applications for environmental purification. *J. Photochem. Photobiol. C Photochem. Rev.* **2012**, *13*, 247–262. [[CrossRef](#)]
11. Hodgson, A.T.; Destaillets, H.; Sullivan, D.P.; Fisk, W.J. Performance of ultraviolet photocatalytic oxidation for indoor air cleaning applications. *Indoor Air* **2007**, *17*, 305–316. [[CrossRef](#)] [[PubMed](#)]
12. Serhane, Y. Continuous air purification by front flow photocatalytic reactor: Modelling of the influence of mass transfer step under simulated real conditions. *Chemosphere* **2022**, *295*, 133809. [[CrossRef](#)] [[PubMed](#)]
13. Hou, T.; Du, H.; Yang, Z.; Tian, Z.; Shen, S.; Shi, Y.; Yang, W.; Zhang, L. Flocculation of different types of combined contaminants of antibiotics and heavy metals by thermo-responsive flocculants with various architectures. *Sep. Purif. Technol.* **2019**, *223*, 123–132. [[CrossRef](#)]
14. Trabelsi, K.; Hajjaji, A.; Gaidi, M.; Bessais, B.; El Khakani, M.A. Enhancing the photoelectrochemical response of TiO₂ nanotubes through their nanodecoration by pulsed-laser-deposited Ag nanoparticles. *J. Appl. Phys.* **2017**, *122*, 064503. [[CrossRef](#)]
15. Hajjaji, A.; Jemai, S.; Rebhi, A.; Trabelsi, K.; Gaidi, M.; Alhazaa, A.N.; Al-Gawati, M.A.; El Khakani, M.A.; Bessais, B. Enhancement of photocatalytic and photoelectrochemical properties of TiO₂ nanotubes sensitized by SILAR—Deposited PbS nanoparticles. *J. Mater.* **2020**, *6*, 62–69. [[CrossRef](#)]
16. Hajjaji, A.; Jemai, S.; Trabelsi, K.; Kouki, A.; Ben Assaker, I.; Ka, I.; Gaidi, M.; Bessais, B.; El Khakani, M.A. Study of TiO₂ nanotubes decorated with PbS nanoparticles elaborated by pulsed laser deposition: Microstructural, optoelectronic and photoelectrochemical properties. *J. Mater. Sci. Mater. Electron.* **2019**, *30*, 20935–20946. [[CrossRef](#)]
17. Wu, Y.; Chen, X.; Cao, J.; Zhu, Y.; Yuan, W.; Hu, Z.; Ao, Z.; Brudvig, G.W.; Tian, F.; Jimmy, C.Y.; et al. Photocatalytically recovering hydrogen energy from wastewater treatment using MoS₂@TiO₂ with sulfur/oxygen dual-defect. *Appl. Catal. B Environ.* **2022**, *303*, 120878. [[CrossRef](#)]
18. Dimitrakopoulou, D.; Rethemiotaki, I.; Frontistis, Z.; Xekoukoulotakis, N.P.; Venieri, D.; Mantzavinos, D. Degradation, mineralization and antibiotic inactivation of amoxicillin by UV-A/TiO₂ photocatalysis. *J. Environ. Manag.* **2012**, *98*, 168–174. [[CrossRef](#)] [[PubMed](#)]
19. Karoui, S.; Ben Arfi, R.; Mougin, K.; Ghorbal, A.; Assadi, A.A.; Amrane, A. Synthesis of novel biocomposite powder for simultaneous removal of hazardous ciprofloxacin and methylene blue: Central composite design, kinetic and isotherm studies using Brouers-Sotolongo family models. *J. Hazard. Mater.* **2020**, *387*, 121675. [[CrossRef](#)] [[PubMed](#)]
20. Assadi, A.A.; Bouzaza, A.; Lemasle, M.; Wolbert, D. Acceleration of Trimethylamine Removal Process Under Synergistic Effect of Photocatalytic Oxidation and Surface Discharge Plasma Reactor. *Can. J. Chem. Eng.* **2015**, *93*, 1239–1246. [[CrossRef](#)]
21. Yanagida, B.S.; Yajima, T.; Takei, T.; Kumada, N. Removal of hexavalent chromium from water by Z-scheme photocatalysis using TiO₂ (rutile) nanorods loaded with Au core–Cu₂O shell particles. *J. Environ. Sci.* **2022**, *115*, 173–189. [[CrossRef](#)] [[PubMed](#)]
22. Kenfoud, H.; Nasrallah, N.; Baaloudj, O.; Derridj, F.; Trari, M. Enhanced photocatalytic reduction of Cr(VI) by the novel hetero-system BaFe₂O₄/SnO₂. *J. Phys. Chem. Solids* **2022**, *160*, 110315. [[CrossRef](#)]
23. Baaloudj, O.; Nasrallah, N.; Assadi, A.A. Facile synthesis, structural and optical characterizations of Bi₁₂ZnO₂₀ sillenite crystals: Application for Cefuroxime removal from wastewater. *Mater. Lett.* **2021**, *304*, 130658. [[CrossRef](#)]

24. Zeghioud, H.; Khellaf, N.; Amrane, A.; Djelal, H.; Elfalleh, W.; Assadi, A.A.; Rtimi, S. Photocatalytic performance of TiO₂ impregnated polyester for the degradation of Reactive Green 12: Implications of the surface pretreatment and the microstructure. *J. Photochem. Photobiol. A Chem.* **2017**, *346*, 493–501. [[CrossRef](#)]
25. Wang, F.-Y.; Yang, Q.-D.; Xu, G.; Lei, N.g.a.i.-Y.; Tsang, Y.K.; Wong, N.-B.; Ho, J.C. Highly active and enhanced photocatalytic silicon nanowire arrays. *Nanoscale* **2011**, *3*, 3269–3276. [[CrossRef](#)]
26. Waterhouse, G.I.N.; Bowmaker, G.A.; Metson, J.B. Oxidation of a polycrystalline silver foil by reaction with ozone. *Appl. Surf. Sci.* **2001**, *183*, 191–204. [[CrossRef](#)]
27. Zhang, Q.; Thrithamarassery Gangadharan, D.; Liu, Y.; Xu, Z.; Chaker, M.; Ma, D. *Recent Advancements in Plasmon-Enhanced Visible Light-Driven Water Splitting*; Elsevier Ltd.: Amsterdam, The Netherlands, 2017; Volume 3, ISBN 4509298102.
28. Song, L.; Luo, L.; Song, J.; Zhang, H.; Li, X.; Cheng, S.; Jin, W.; Tang, J.; Liu, L.; Wang, F. Enhanced Photodegradation Activity of Hydrogen-Terminated Si Nanowires Arrays with Different-Oriented Crystal Phases. *Catalysts* **2017**, *7*, 371. [[CrossRef](#)]
29. Nishanthi, S.T.; Iyyapushpam, S.; Sundarakannan, B.; Subramanian, E.; Pathinettam Padiyan, D. Plasmonic silver nanoparticles loaded titania nanotube arrays exhibiting enhanced photoelectrochemical and photocatalytic activities. *J. Power Sources* **2015**, *274*, 885–893. [[CrossRef](#)]
30. Li, C.; Lin, H.; Armutlulu, A.; Xie, R.; Zhang, Y.; Meng, X. Hydroxylamine-assisted catalytic degradation of ciprofloxacin in ferrate/persulfate system. *Chem. Eng. J.* **2019**, *360*, 612–620. [[CrossRef](#)]
31. Kenfoud, H.; Nasrallah, N.; Meziani, D.; Trari, M. Photoelectrochemical study of the spinel CaFe₂O₄ nanostructure: Application to Basic Blue 41 oxidation under solar light. *J. Solid State Electrochem.* **2021**, *25*, 1815–1823. [[CrossRef](#)]
32. Zeghioud, H.; Assadi, A.A.; Khellaf, N.; Djelal, H.; Amrane, A.; Rtimi, S. Photocatalytic performance of Cu_xO/TiO₂ deposited by HiPIMS on polyester under visible light LEDs: Oxidants, ions effect, and reactive oxygen species investigation. *Materials* **2019**, *12*, 412. [[CrossRef](#)] [[PubMed](#)]
33. Azzaz, A.A.; Jellali, S.; Assadi, A.A.; Bousselmi, L. Chemical treatment of orange tree sawdust for a cationic dye enhancement removal from aqueous solutions: Kinetic, equilibrium and thermodynamic studies. *Desalin. Water Treat.* **2016**, *57*, 22107–22119. [[CrossRef](#)]
34. Herrmann, J.M.; Tahiri, H.; Guillard, C.; Pichat, P. Photocatalytic degradation of aqueous hydroxy-butandioic acid (malic acid) in contact with powdered and supported titania in water. *Catal. Today* **1999**, *54*, 131–141. [[CrossRef](#)]
35. Zadi, T.; Assadi, A.A.; Nasrallah, N.; Bouallouche, R.; Tri, P.N.; Bouzaza, A.; Azizi, M.M.; Maachi, R.; Wolbert, D. Treatment of hospital indoor air by a hybrid system of combined plasma with photocatalysis: Case of trichloromethane. *Chem. Eng. J.* **2018**, *349*, 276–286. [[CrossRef](#)]
36. Akpan, U.G.; Hameed, B.H. Parameters affecting the photocatalytic degradation of dyes using TiO₂-based photocatalysts: A review. *J. Hazard. Mater.* **2009**, *170*, 520–529. [[CrossRef](#)] [[PubMed](#)]
37. Pereira, J.H.O.S.; Reis, A.C.; Queirós, D.; Nunes, O.C.; Borges, M.T.; Vilar, V.P.; Boaventura, R.A.R. Insights into solar TiO₂-assisted photocatalytic oxidation of two antibiotics employed in aquatic animal production, oxolinic acid and oxytetracycline. *Sci. Total Environ.* **2013**, *463–464*, 274–283. [[CrossRef](#)]
38. Dionysiou, D.D.; Suidan, M.T.; Bekou, E.; Baudin, I.; Laïné, J.M. Effect of ionic strength and hydrogen peroxide on the photocatalytic degradation of 4-chlorobenzoic acid in water. *Appl. Catal. B Environ.* **2000**, *26*, 153–171. [[CrossRef](#)]
39. Malato, S.; Fernández-Ibáñez, P.; Maldonado, M.I.; Blanco, J.; Gernjak, W. Decontamination and disinfection of water by solar photocatalysis: Recent overview and trends. *Catal. Today* **2009**, *147*, 1–59. [[CrossRef](#)]
40. Gerischer, H.; Heller, A. The role of oxygen in photooxidation of organic molecules on semiconductor particles. *J. Phys. Chem.* **1991**, *95*, 5261–5267. [[CrossRef](#)]
41. Zeghioud, H.; Assadi, A.A.; Khellaf, N.; Djelal, H.; Amrane, A.; Rtimi, S. Reactive species monitoring and their contribution for removal of textile effluent with photocatalysis under UV and visible lights: Dynamics and mechanism. *J. Photochem. Photobiol. A Chem.* **2018**, *365*, 94–102. [[CrossRef](#)]
42. Baaloudj, O.; Nasrallah, N.; Kebir, M.; Khezami, L.; Amrane, A.; Assadi, A.A. A comparative study of ceramic nanoparticles synthesized for antibiotic removal: Catalysis characterization and photocatalytic performance modeling. *Environ. Sci. Pollut. Res.* **2020**, *28*, 13900–13912. [[CrossRef](#)] [[PubMed](#)]